

RFI MITIGATION IN THE CONTEXT OF PULSAR COHERENT DE-DISPERSION AT THE NANCAY RADIO ASTRONOMICAL OBSERVATORY

D. Ait allal¹, R. Weber², I. Cognard^{1,3}, G. Desvignes³ and G. Theureau^{1,3,4}

¹Station de radioastronomie de Nançay, Observatoire de Paris, CNRS/INSU Nançay, F-18300 Nançay, France
dalal.ait-allal@obs-nancay.fr

²Institut PRISME – Université d'Orléans 12 Rue de Blois BP 6744 Orléans Cedex 2 F-45067 France,
rodolphe.weber@univ-orleans.fr

³Laboratoire de Physique et Chimie de l'Environnement et de l'Espace, UMR 6115 CNRS, F-45071 Orléans Cedex 02, France,
icognard@cnrs-orleans.fr, Gregory.Desvignes@cnrs-orleans.fr

⁴GEPI, Observatoire de Paris, CNRS, Université Paris Diderot ; Place Jules Janssen 92190 Meudon, France, theureau@cnrs-orleans.fr

ABSTRACT

Radio astronomical pulsar observations require specific instrumentation and dedicated signal processing to cope with the dispersion caused by the interstellar medium. Moreover, the quality of observations can be limited by radio frequency interferences (RFI) generated by Telecommunications activity. This paper will present the innovative pulsar instrumentation based on Graphical Processing Units (GPU) which has been designed at the Nançay Radio Astronomical Observatory. In addition, first simulated results on RFI cyclostationary detectors, which will be implemented on the system, will be described and discussed.

1. CONTEXT

The radio astronomy is a field that uses radio waves emitted by celestial objects for astronomic observations and studies. Among those fascinating objects, pulsars – rapidly rotating highly magnetized neutron stars - produce radio beams that sweep the sky like a lighthouse [1]. If the beam is oriented towards the Earth, it will produce periodic pulses which can be measured with radio telescopes and dedicated backends. During their travel through the interstellar medium (ISM), these pulses are progressively attenuated and spread over time (i.e. pulse higher frequencies will arrive earlier than the pulse lower frequencies). Figure 1.a and 1.b shows a raw time-frequency representation of one of these pulses. This phenomenon, named dispersion, makes these pulses barely detectable without further processing. Moreover, the quality of pulsar observations is also limited by radio frequency interferences (RFI) generated by various (and growing) Telecommunications activities. Figure 2 gives an example of the distortion induced by RFI on pulsar observation.

To invert the ISM effect, specific receiver must be designed, and to limit the impact of RFI, robust signal processing algo-

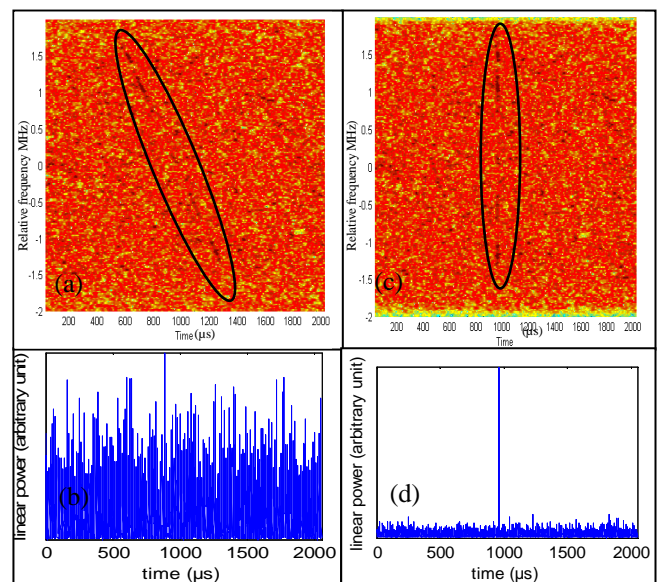


Figure 1–a. Time-frequency representation of a giant pulse from the Crab (PSR 0531+21) as it is measured without further processing. b. Corresponding power fluctuations over time in the 4 MHz band. The pulse is undetectable c. Time-frequency representation of the same giant pulse after de-dispersion. d. Corresponding power fluctuations over time in the 4 MHz band. The pulse is easily detectable.

gorithms must be applied. This paper will present an original backend which has been designed for pulsar de-dispersion and simulations of RFI mitigation techniques which can be applied in such context.

In section 2, the functional description of the coherent de-dispersion algorithm is explained and the innovative hardware architecture of the Nançay de-dispersion backend is detailed. In section 3, a waveform pulsar model is derived. This model will be used to test RFI mitigation algorithms. Their description and their simulation are given in section 4.

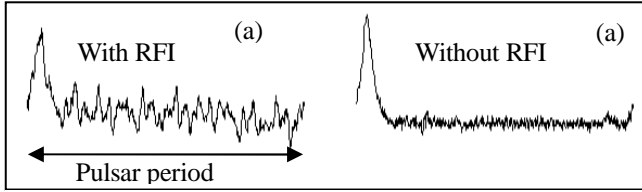


Figure 2 – a. Time representation of the average power pulse profile of the pulsar J0034-0721 after coherent de-dispersion but with RFI signals. b. Time representation of the average power pulse profile of the pulsar J0034-0721 after coherent de-dispersion and with RFI signals blanked (with other RFI mitigation Scheme).

2. NANÇAY INSTRUMENTATION FOR PULSAR OBSERVATIONS

2.1 Coherent de-dispersion principle

The ISM dispersion can be modelled as a frequency transfer function [1], H :

$$H(f_0 + f) = e^{+j \frac{2\pi DM}{2.41 \times 10^{-10}} (f + f_0) f_0^2} \quad (1)$$

Where DM is the dispersion measure, f_0 is the center frequency of observed bandwidth Δf and $|f| < \Delta f/2$.

The coherent de-dispersion consists of applying the inverse of this transfer function to the dispersed received signal. This processing is done in the frequency domain by using Fourier transforms. The operations are detailed inside the “Data server” box in Figure 3. The taper function is used to avoid aliasing in the low-pass filtering. The combination of the inverse of the dispersion transfer function and the taper function is known as the chirp function.

2.2 Hardware Implementation

Figure 3 shows the signal dataflow from the radio telescope to the final de-dispersed pulses. The different steps are described below:

- The Analog System [2]: two orthogonal polarization signals from the radio telescope are downconverted through a custom circuit board quadrature downconverter (QDC). Each QDC handles one polarization and performs a quadrature demodulation providing 128 MHz complex bandwidth which is sent to the SERENDIP5 Spectrometer for digitalisation and channelizing.
- The SERENDIP5 Spectrometer [2]: SERENDIP5 (Search for Extraterrestrial Radio Emissions from Nearby Developed Intelligent Populations) was designed by CASPER (Center For Astronomy Signal Processing and Electronics Research) for applications in SETI (Search for Extra-Terrestrial Intelligence), Pulsar and general radio astronomy. For this application, it contains four 8-bit analog to digital converters (ADCs) that can be clocked up to 200MHz. A logic programmable device (Virtex 2 XC2V4000 from Xilinx) is used to perform a 32 channel polyphase filter bank (PFB). The channel output bandwidth is 4 MHz complex. An addi-

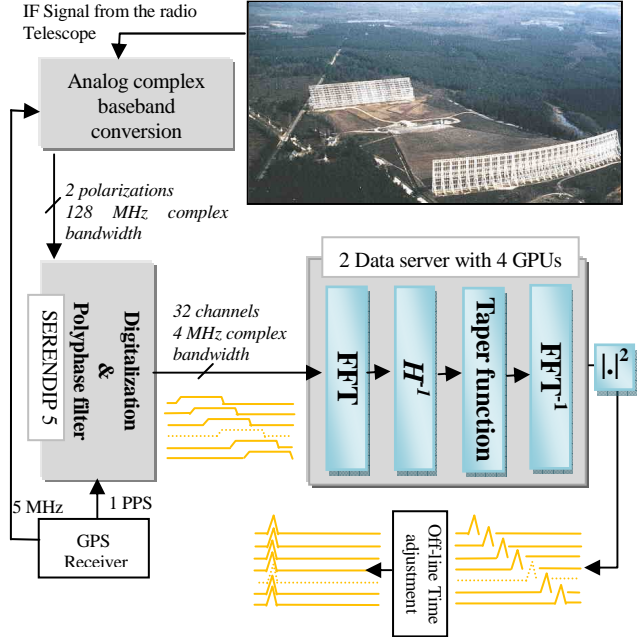


Figure 3 – Description of the instrumentation for pulsar observations which is in operation since July 2008 at Nançay Observatory. The top right hand corner picture is the giant decimetre radio telescope of Nançay.

tional Xilinx device (Virtex 2 XC2V1000) is used as a reconfigurable backend processor which can pass data to an independent computer

- Data servers: This is the innovative part of the design. The two data servers have two main processing’s steps. The first one is to read the raw data in from the SERENDIP5 spectrometer and reorganize them from a channel-order to single-channel time ordered chunks. This step is controlled by four micro processors, that send these chunks to four GPUs [3] (Graphic Processing Unit- NVIDIA 88 GTX ~128 parallel processors) for the final processing’s step. The data are then read by the de-dispersion program that performs the following tasks:
 - Convert raw data from binary to floating point.
 - Apply a Fourier transform of appropriate length (8192 bins).
 - Multiply by the de-dispersion filter, H^{-1} and the taper function
 - Inverse Fourier transform back to the time domain.
 - Detect the data to get power versus time, and cross-multiply polarization terms.
- Time adjustment: offline resynchronisation of all the channels.
- GPS receiver: It provides SERENDIP5 clock synchronization through a one pulse per second (1PPS) signal and oscillator synchronization through a 5 MHz reference clock.

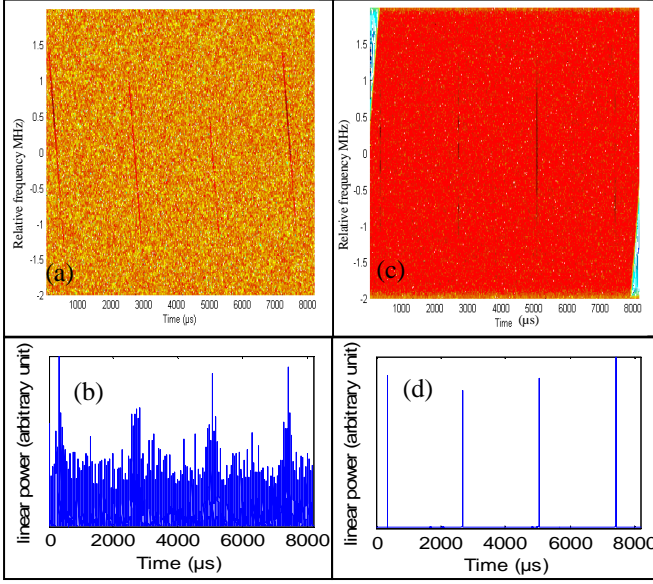


Figure 4 – **a.** Time-frequency representation of the pulsar signal generated by the model given by Equ. 7 ($BW=4\text{MHz}$, $t_{DM}=938.0793\ \mu\text{s}$ and pulsar period is $2.35\ \text{ms}$). **b.** Corresponding temporal power fluctuations over the whole bandwidth. **c.** Time-frequency representation after de-dispersion. Equ. 1 has been used with the following parameters $f_0=1262\ \text{MHz}$ and $DM=56.791\ \text{pc.cm}^{-3}$. **d.** Corresponding temporal power fluctuations over the whole bandwidth.

This coherent de-dispersion pulsar receiver is operational since July 2008 at Nançay Observatory [4]. Figure 1.c gives the result of this coherent de-dispersion applied on the signal from Figure 1.a. We can see that after the coherent de-dispersion, the pulse is no more spread and its power can be easily detected (Figure 1.d compared to Figure 1.b).

To improve the system sensitivity and its robustness to RFI, it is planned to implement RFI mitigation algorithms in this system. The next sections will describe the preliminary simulated results obtained on that topic.

3. PULSAR SIGNAL MODEL

In our model, we assume that the pulsar beam is represented by periodic Dirac impulsions so that the pulse signal can be modelled as successive chirp functions.

The temporal evolution of the frequency can be written as:

$$f(t) = \frac{\alpha BW}{t_{DM}^2} t^2 - \frac{BW(\alpha+1)}{t_{DM}} t + \frac{BW}{2}, \quad t \in [0, t_{DM}] \quad (2)$$

where BW is the bandwidth (typically $4\ \text{MHz}$), t_{DM} is the dispersion delay over this bandwidth, α is a factor which characterises second order delay distortions. Without loss of generality, all the simulations have been made with $\alpha=0$ (i.e. the frequency becomes a linear function of time). Thus, Equ. (2) becomes:

$$f(t) = -\frac{BW}{t_{DM}} t + \frac{BW}{2}, \quad t \in [0, t_{DM}] \quad (3)$$

Then, the phase of the pulsar signal can be expressed as

$$\phi(t) = 2\pi \left(-\frac{BW}{2t_{DM}} t^2 + \frac{BW}{2} t \right), \quad t \in [0, t_{DM}] \quad (4)$$

Finally, the time representation of the pulse shape within its period number k is expressed by:

$$v_k(t) = A_k(t) e^{j(\phi(t)+\theta_k)} \quad \text{for } t \in [0, t_{DM}] \\ v_k(t) = 0 \quad \text{otherwise} \quad (5)$$

where $\phi(t)$ is defined by Equ. (4), T_p is the pulsar period, θ_k is a random phase and $A_k(t)$ is a random amplitude which represents the scintillation effects. Indeed, inhomogeneities in the ISM cause multi-path propagation which produces interference of the signals and diffraction pattern. As a result, we observe changes in intensity with both frequency and time.

The quadratic term in Equ. (4) is directly related to the dispersion function defined by Equ. (1) if we consider also linear frequency shift over the bandwidth (i.e. $f_0 \gg \Delta f$). So, we will use the same de-dispersion algorithm as for real pulsar signal.

Figure 4 shows an example of a generated pulsar and the result after de-dispersion. Results are the one expected. With this model, we can generate all kind of scenario to test our RFI mitigation algorithms. Next subsection will present a first algorithm based on the cyclostationary properties of RFI.

4. RFI CYCLOSTATIONNARY DETECTOR AND THE INTEREST OF BLANKING

The proposed detector is based on RFI specific properties named cyclostationarity. Indeed, most of telecommunications signals present a hidden periodicity which is usually scrambled by the intrinsic signal randomness [5,6]. For example, this hidden periodic characteristic can be generated by the carrier frequency or the baud rate of the incoming RFI.

3.4 Cyclostationary detector principle

In [7], we have defined and study the statistics of a cyclostationary detector based on the following criteria:

$$C_{s^{(*)}}^\alpha = \left| \frac{1}{N} \sum_{n=0}^N s(n) s(n)^{(*)} e^{-2\pi\alpha n} \right| \quad (6)$$

Where α is the frequency related to the hidden periodicity (α is also called the cyclic frequency), $s(n)$ is a signal to be controlled and $*$ is the conjugate operator which may be used or not. C_s^α and $C_{s^{(*)}}^\alpha$ are called respectively the conjugate cyclostationary detector and the cyclostationary detector.

Asymptotically, if $s(n)$ is stationary, $C_{s^{(*)}}^\alpha$ will be null. Otherwise, if $s(n)$ is cyclostationary with cyclic frequency α , then $C_{s^{(*)}}^\alpha$ will be non zero. Notice that $C_{s^{(*)}}^0$ is simply a power detector.

We have also defined normalized detection criterion:

$$D_{s^{(*)}}^\alpha = \frac{C_{s^{(*)}}^\alpha}{C_{s^{(*)}}^0} \quad (7)$$

If the cyclic frequency to be detected is not known, we can implement blind cyclic detectors by testing all cyclic frequencies. This can be easily done through FFTs. If the cyclic frequency does not map strictly the FFT bins, the detectors will lose a maximum of 3db in term of sensitivity [7].

In practice, the detectors are applied on a sliding temporal window of N samples. If detection occurs, the whole N samples are flagged as polluted. Depending on the RFI strategy, these N samples can be blanked (i.e. replace by 0) or not.

3.5 Simulation and results

For the simulation, we have considered a BPSK (Binary Phase Shift keying) RFI:

$$rfi(t) = \sum_k a_k h(t - kT_d) e^{i(2\pi f_c t + \varphi)} \quad (8)$$

where f_c is the carrier frequency, $1/T_d$ is the baud rate, a_k is a random binary signal, $h(t)$ is the emission filter and φ is a random phase.

Theoretically, in the case, the cyclic frequencies are $\alpha = n/T_d$, $n \in \mathbb{Z}$ for the $C_{S^*}^\alpha$ detector and $\alpha = 2f_c + n/T_d$, $n \in \mathbb{Z}$ for the C_S^α detector. Figure 5 shows the detector values as a function of the cyclic frequency. In this example, we retrieve the above theoretical cyclic frequencies. It shows also that the conjugate cyclostationary detector with $\alpha = 2f_c$ is the most contrasted criteria.

The generated signal will have the following structure:

$$s(t) = \sum_k v_k(t - kT_p) + rfi(t) + n(t) \quad (9)$$

Where $v_k(t)$ is defined by Eq. (7), T_p is the pulsar period, $rfi(t)$ is defined by Eq. (8), and $n(t)$ is a complex Gaussian noise.

Let us also define the interference to noise ratio

$$INR_{dB} = 10 \log_{10} \left(\frac{P_{rfi}}{P_{noise}} \right) \quad (10)$$

Where, P_{rfi} and P_{noise} are the total power of respectively the RFI and system noise.

In addition, we define the pulse signal to noise ratio as

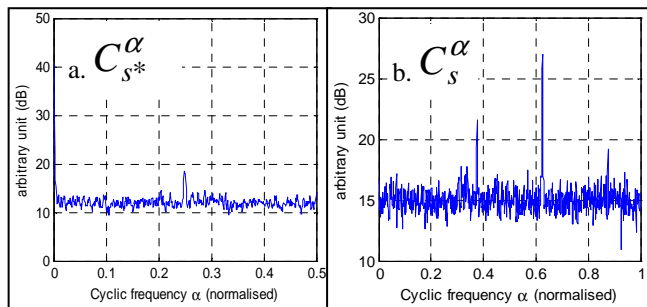


Figure 5 – Cyclic frequency measurements on the simulated BPSK signal with the following parameters $f_c = 0.3125 F_s$ and $T_d = 4/F_s$ (F_s is the sampling frequency). The INR_{dB} has been set to 5 dB. **a.** the cyclostationary detector $C_{S^*}^\alpha$ **b.** the conjugate cyclostationary detector C_S^α . The conjugate cyclostationary detector with $\alpha = 2f_c$ is the most contrasted criteria.

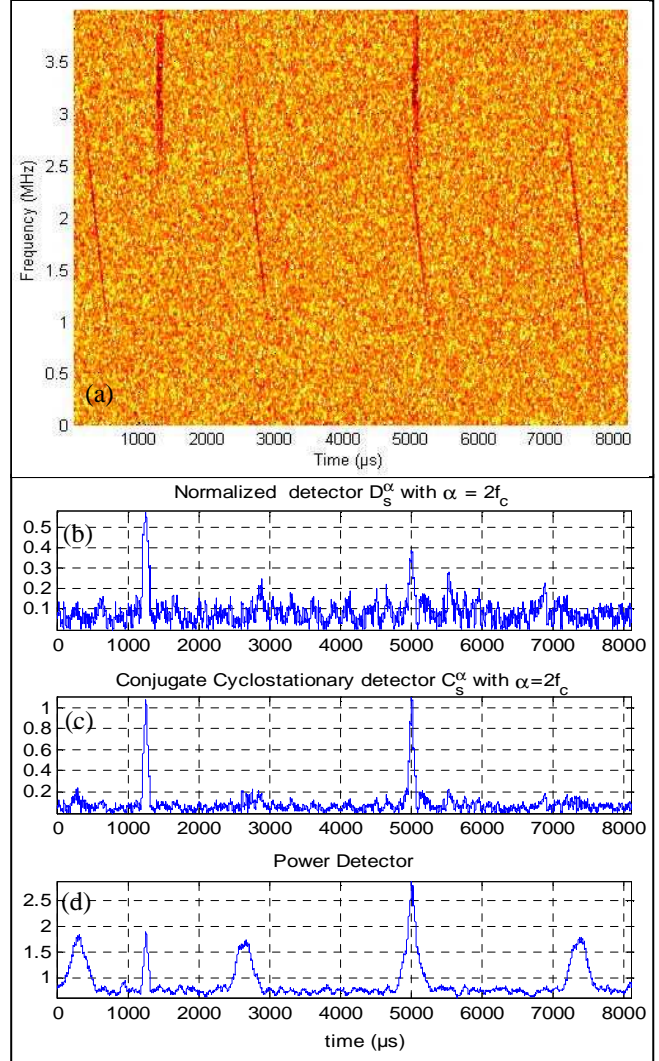


Figure 6 – Detection of impulsive or burst broadband RFI signals by using the conjugate cyclostationary detector **a.** Time-frequency representation of the pulsar signal generated by the model given by Eq. 7 ($BW=4\text{MHz}$, $t_{DM}=938.0793 \mu s$ and pulsar period is 2.35 ms, $RSB= -1 \text{ dB}$) and 2 short BPSK RFI signals generated with Eq. 10 (duration= $80\mu s$, $f_c=25 \text{ kHz}$, $T_d=0.5\mu s$, $h(t)$ is root raised cosine filter with roll-off equal to 1 $INR=3\text{dB}$). **b.** the normalized conjugate cyclostationary detector over time ($N=256$ samples), **c.** The conjugate cyclostationary detector ($N=256$ samples). **D.** the Power detector ($N=256$ samples).

$$SNR_{dB} = 10 \log_{10} \left(\frac{P_{pulses}}{P_{noise}} \right) \quad (11)$$

Where, P_{pulses} is the total power of the Pulsar's pulses.

The results, in figure 6, show that the cyclostationary detector detects only the bursts. While the power detector cannot make the difference between bursts and Pulsar's pulses.

The next step is to decide to eliminate the RFI or not, taking into account the impact of this decision on the quality of the waveform of the pulsar, or other characteristic which may be distorted. See Figure 7.

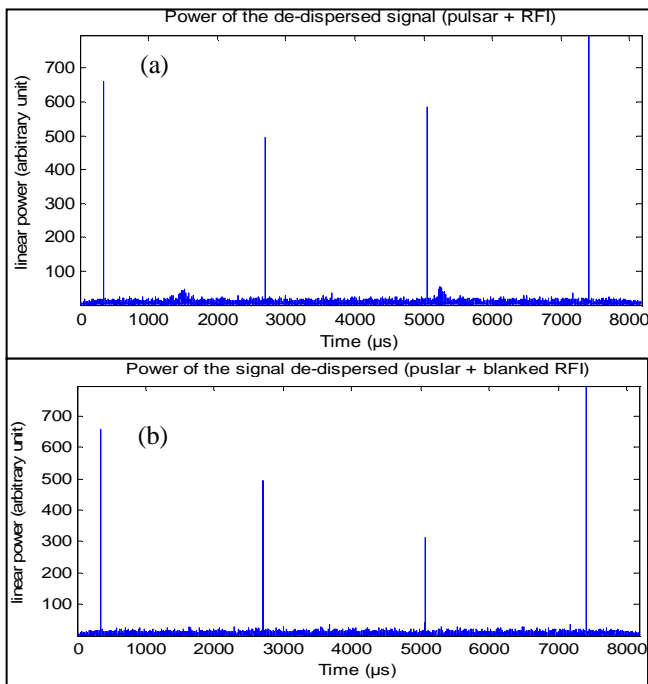


Figure 7 – Blanking of impulsive or burst broadband RFI signals. **b.** Temporal power fluctuations over the whole bandwidth without detection and blanking. **c.** Temporal power fluctuations over the whole bandwidth with detection and blanking. The RFI signals have been removed. Since a part of the 3rd pulse energy is also blanked, the power level of this 3rd pulse is modified.

Depending on where these detectors will be implemented in the system, different type of RFI can be detected. Three possibilities have been identified on the system architecture defined on Figure 2:

(A) at the input of the polyphase filter bank, just after the digitalisation. This configuration is appropriate for impulsive or burst broadband RFI. Figure 6 and Figure 7 shows a simulated example of detection and blanking in such configuration. The power detector will detect pulsar pulses and RFI pulses. The conjugate cyclic detector will only detect the RFI.

(B) Just after the polyphase filter bank.

(C) Just after the FFT, in the coherent de-dispersion process.

This configuration is appropriate for narrow band and continuous RFI.

5. CONCLUSIONS

In the context of pulsar observation, a processing architecture based on 4 Graphic Processing Unit (GPU board) has been presented. This system performs the real time coherent de-dispersion process. It is now fully operational at Nançay Observatory and it outperforms the performances of the previous system based on a cluster of 77 bi-processor Athlon 1.2 GHz. The next step will be to integrate real time RFI detectors. By simulation, we have shown that cyclostationary detectors can be a very interesting alternative to power detectors.

REFERENCES

- [1] D. Lorimer and M. Kramer, *Handbook of Pulsar Astronomy*. Cambridge, United Kingdom: Cambridge University Press, 2005.
- [2] Paul B. Demorest, "Measuring the Gravitational Wave Background using Precision Pulsar Timing," *thesis*, Chapter 3, University of California, Berkeley. Spring. 2007.
- [3] <http://www.cv.nrao.edu/~pdemores/gpu/>
- [4] <http://www.obs-nancay.fr/>
- [5] E. Serpedin, F. Panduru, I. Sari, and G.B. Giannakis, "Bibliography on cyclostationarity," *Signal Processing*, vol. 85, Dec. 2005, pp. 2233-2303.
- [6] W.A. Gardner, A. Napolitano, and L. Paura, "Cyclostationarity: Half a century of research," *Signal Processing*, vol. 86, Apr. 2006, pp. 639-697
- [7] R. Weber , P. Zarka , V. B. Ryabov , R. Feliachi , J.M. Grießmeier , L. Denis, R. V. Kozhyn, V. V. Vinogradov, P. Ravier, " Data pre-processing for decametre wavelength exoplanet detection: An example of cyclostationary RFI detector," in *Proc. EUSIPCO 2007*, Poznan, Poland, September 3-7. 2007.